Research Article ISSN 2769-6294

International Journal of Biomedical Research & Practice

Limited-Angle Tomography Using a Neural Network as the Objective Function

Gengsheng L Zeng*

Department of Computer Science, Utah Valley University, Orem, USA.

***Correspondence:**
Gengsheng L Zeng, Department of Computer Science, Utah Valley University, Orem, USA, Tel: 18018638306.

Received: 13 Jun 2025; **Accepted:** 21 Jul 2025; **Published:** 30 Jul 2025

Citation: Gengsheng L Zeng. Limited-Angle Tomography Using a Neural Network as the Objective Function. Int J Biomed Res Prac. 2025; 5(1); 1-9.

ABSTRACT

In limited-angle tomography, the system of imaging equations is underdetermined, and a naïve reconstruction may not have any practical values. Additional information is needed to augment the data so that a useful image can be reconstructed. This additional information is usually implemented as a Bayesian term in the objective function for an iterative optimization procedure. The state-of-the-art augmented information is the total variation (TV) norm of the image. The TV norm enforces a smooth image with sharp edges. The novelty of this paper is a new Bayesian term that is in the form of a neural network. This neural network is a classifier trained by images reconstructed by full and limited-angle projections. The impact of the proposed method is that the information provided by the neural network contains more features of the images than the TV norm and better reconstruction is expected. Computer simulations are carried out and presented.

Keywords

Tomography, Optimization, Inverse problem, Under-sampled data, Limited-angle tomography, Image reconstruction, Convolutional neural network, Classifier, Bayesian.

Abbreviations

CNN: Convolutional neural network**,** FBP: Filtered backprojection**,** TV: Total variation**.**

Introduction

Data sufficiency conditions have been well established for imaging modalities and geometries [1]. If the data sufficiency conditions are satisfied, stable image reconstruction algorithms exist. Due to many practical constraints such as camera size, object size, and trajectory obstacles, the conditions cannot be met. In these situations, the measurements are referred to as incomplete.

In various clinical imaging techniques, incomplete data due to limited-angle or few-view projections can hinder diagnostic accuracy. For example, in dental and C-arm cone-beam imaging [2-7], the camera typically rotates in a circle, already failing to capture a full dataset by violating Tuy's condition [8]. Limited-angle or few-view acquisition only makes the situation worse. In Digital Breast Tomosynthesis (DBT) [9-12], 11 to 49 images are taken from different angles as the X-ray tube moves in an arc over the breast, a scenario known as limited-angle, few-view tomography. While DBT provides critical diagnostic information, its data set is inherently incomplete. Breast CT, which offers higher resolution, is rarely used due to the increased radiation dose, particularly in patients who are young or at high risk.

In intraoperative settings, e.g., spinal tumor resections, C-arm fluoroscopy is employed to verify the position of surgical instruments (e.g., screws, rods). However, during these procedures, the available data often comes from limited-angle imaging or few-view CT. Similarly, cone-beam CT is utilized in image-guided radiation therapy (IGRT) to assist with precise targeting during radiotherapy treatments [13,14]. In these cases, when only a limited number of views are accessible such as in lung cancer treatments, where respiratory motion complicates positioning, advanced reconstruction techniques are crucial to maintain image quality. Few-view imaging has proven beneficial in cases where

tumor access is constrained or where the patient's positioning makes full-angle imaging impossible [15-19]. This is particularly true in image-guided breast cancer surgery, where limited-angle imaging is frequently required due to the patient's body position.

Emergency departments often face situations where full-angle imaging cannot be achieved due to patient instability or inability to reposition. In these cases, few-view scans are critical for rapid assessment of conditions like fractures, internal bleeding, or organ damage. In spinal surgeries, interventional oncology, or trauma care, the limitations on imaging angles may necessitate specialized reconstruction methods to achieve clinically useful images.

A key challenge in these applications is minimizing radiation exposure, especially in pediatric patients, individuals requiring repeated imaging, and cancer patients undergoing radiotherapy. Adhering to the "As Low As Reasonably Achievable" (ALARA) principle ensures that radiation doses are minimized while still providing necessary clinical information [20-28]. Adhering to the "As Low as Reasonably Achievable" (ALARA) principle ensures that radiation doses are minimized while still providing necessary clinical information [20-28]. Few-view tomography offers a promising solution. However, the resulting images often suffer from artifacts due to the incomplete data set. Thus, developing methods to mitigate these artifacts is a critical area of focus for this proposal.

In the field of medical imaging, such as x-ray computed tomography (CT), standard protocols usually guarantee that the data collected is sufficient for accurate image reconstruction. The conditions required to obtain a complete data set are well defined. These include Tuy's condition for cone beam imaging geometry [8]. However, in practical scenarios, these conditions may be violated due to various constraints such as the structure and size of the camera, the movement trajectory during imaging, metal obstruction, and restrictions on imaging time. These violations lead to incomplete data sets, which complicate the image reconstruction process and may introduce artifacts in the reconstructed images.

Here is the current understanding of why incomplete data may cause artifacts and how to reduce them. The first-order approximation of the measurements in tomographic imaging can be represented as a system of linear equations, commonly referred to as the imaging equations [29-34]. The first-order approximation of measurements in tomographic imaging can be represented as a system of linear equations, commonly referred to as the imaging equations [29-34]. In these equations, the unknowns are the values of the image pixels. When the data sufficiency conditions are not met, the system of imaging equations becomes underdetermined. This means there are more unknowns than equations, making the problem of image reconstruction extremely ill-conditioned [35-41].

In an ill-conditioned problem, a small deviation in the input data can lead to large variations in the output, making the reconstruction process highly sensitive to errors. Even in a noiseless situation, the solution is not unique. This is a significant challenge in medical imaging, as accurate and reliable images are crucial for diagnosis and treatment planning.

To address the issue of ill-conditioning, regularization techniques are employed. Regularization introduces additional information or constraints to stabilize and restrict the solution to a desired category. The theoretically ideal regularization method is the use of the L_0 norm minimization, which is suggested by compressed sensing methodology when the image, or a transformed version of it, is sparse [42-58]. Sparsity implies that most of the image pixels are zero. The L_0 norm counts the number of non-zero pixels in the image. However, the L_0 norm is difficult to use in optimization algorithms due to its derivative being zero almost everywhere, making it challenging to implement effectively. The total variation (TV) norm measures the total change in intensity across the image, which is the L_1 norm of the image gradients. TV norm optimization is a good substitution for L_0 norm optimization and has become the state-of-the-art technique [59-70]. TV regularization has limitations. It primarily measures the total change and does not give special priority to piecewise constant functions.

Machine learning has revolutionized numerous fields, including medical imaging. One of the remarkable capabilities of neural networks is their ability to transform images with artifacts into clear, patient-like images [71-94]. However, this powerful tool comes with significant responsibilities. When the measurements used to create these images are incomplete, the neural network-generated images may contain hallucinations, which do not correspond to actual patient data [95-100]. These hallucinations can mislead medical diagnoses, potentially causing harm. The hallucinations may be caused by limited data, noise, wrong assumptions made by the reconstruction algorithms, or the deep-learning models.

To ensure the reliability of reconstructed images from under-sampled data, it is crucial that the final image is primarily determined by the actual measurements. The role of the neural network should be limited to providing regularization, rather than generating the image itself. In this context, we do not assume that the image, or any transformed version of it, is sparse.

Our approach involves using the patient population to develop a neural network that functions as a classifier. This classifier will produce a continuous output rather than a binary one. A smaller output value will indicate that the image is closer to the typical images found in the patient population. This method aims to ensure that the reconstructed images are as accurate and reliable as possible, even when the data is incomplete. By focusing on the specific properties of piecewise functions, we hope to achieve better regularization and, consequently, higher-quality images in medical tomographic imaging.

To do better than using the TV norm in an objective function, this paper suggests using a neural network as a Bayesian term [101,102]. The motivation of this suggestion is that a neural network can extract more features than the TV norm to identify desired images.

There are many types of neural networks. Some of them are generative. For example, a trained neural network can convert a low-resolution image to a high-resolution image, to remove noise from a noisy image, or to reduce the artifacts from the original image. When measurements are incomplete, the image obtained by the generative network may contain hallucinations, which are some small details not in the original objects. Hallucinations can lead to misinformation and incorrect diagnoses. This is a serious concern, especially in diagnostic imaging. On the other hand, neural network classifiers are more trustworthy and usually have better-than-human performances.

We will use the more reliable iterative image reconstruction to reconstruct the image from the incomplete measurements with a neural network classifier being a Bayesian term in the objective function. In the next section we will explain how a classifier is converted into a Bayesian term.

Methods

Objective Function

The objective function for iterative image reconstruction usually contains a data fidelity term and one or more Bayesian terms.

The data fidelity term is the squared L_2 norm of the distance between the measurements and the forward projections of the reconstructed image.

A typical Bayesian term is the TV norm of the reconstructed image. Here we suggest a new Bayesian term that is calculated by a neural network.

The proposed neural network is a classifier with a slight modification. Let us consider a two-class classifier, which is a deep-convolutional neural network (CNN) followed by a single neuron with a sigmoid activation function. The sigmoid function has two large flat regions, and the derivative of the sigmoid function is almost zero in these regions. A flat objective function term is not desired because it is almost useless in a gradient based optimization algorithm.

This classifier is trained by images reconstructed with full data (label = 0) and images reconstructed with incomplete data (label = 1). After this classifier is trained by a supervised algorithm, we remove the final sigmoid function. We use the trained classifier without the final sigmoid function as a new Bayesian term in the objective function for image reconstruction.

Neural Network Classifier

Any neural network classifier can be used. We randomly selected a with 7 CNN layers with the number of channels as 5, 10, 35, 40, 45, 50 and 1, respectively. At each CNN layer, the convolution kernel size was 3 × 3, strides were 2, activation function was a ReLU (rectified linear unit). Finally, we had a dense neuron. The input image size was 64 × 64. The output was a real scalar. The training images were computer simulated consisting of 50,000 true images and 50,000 images reconstructed with incomplete data. The 'adam' algorithm was used to train the network with the 10 epochs.

Image Reconstruction

An iterative gradient descent algorithm was used to minimize the objective function, which consisted of three terms: the data fidelity term, the TV Bayesian term and the neural network Bayesian term.

The gradients of the neural network output with respect to the image pixels can be readily obtained by using TensorFlow's backpropagation as [103]:

```
with tf.GradientTape() as tape:
  tape.watch(recon_tensor)
output = model(recon_tensor)
grads = tape.gradient(output, recon_tensor)
```

Here recon_tensor is the current reconstructed image tensor, and output is the network output. This snippet tracks how the output changes concerning the recon_tensor.

In TensorFlow, tf.GradientTape is a context manager that records operations for automatic differentiation.

We start the context for recording: with tf.GradientTape() as tape.

We then tell the tape to watch recon_tensor so that it keeps track of all operations involving this tensor for gradient calculation using tape.watch(recon_tensor).

We pass recon_tensor through the model to get the output as output = model(recon_tensor).
Finally, we compute the gradients of output with respect to recon_tensor.

Computer Simulations

We randomly generated some phantom images that were never used in the network training for image reconstruction studies. The phantoms ellipses of random shapes, directions, locations, and intensities.

In one set of studies, the scanning angles covered 60°. In the other set of studies, the scanning angles covered 70°. The number of iterations in image reconstruction was 30,000. The step size for the data fidelity term was 0.01. The step size for the TV term was 0.001. The step size for the network term was 0.2. Projections were parallel beams. For comparison purposes, we also performed the reconstruction with the following methods: non-iterative Filtered Backprojection (FBP) reconstruction, iterative TV reconstruction (by disabling the network Bayesian term), and iterative reconstruction by disabling the TV term.

Results

Eight phantom reconstruction results are presented in Figures 1 to 8. Figures 1 to 4 use projections over 70°. Figures 5 to 8 use projections over 60°.

Scanning angle = 70°

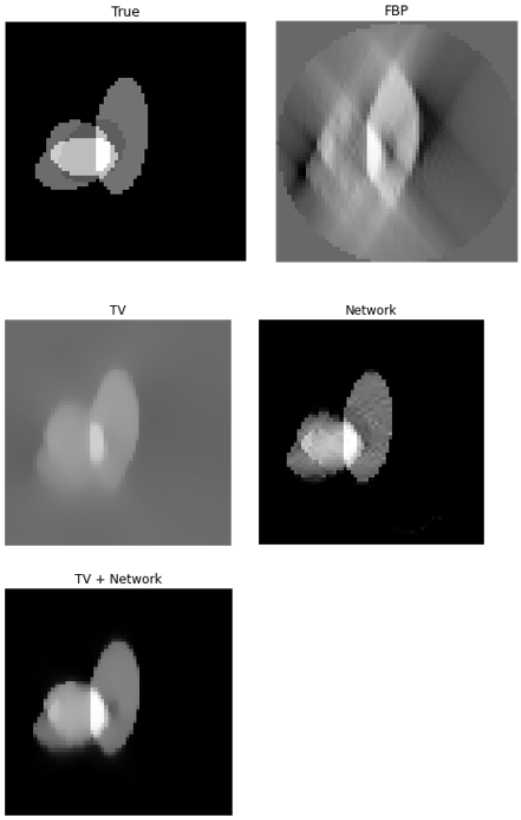

Figure 1: Simulation case 1.
True: True image. FBP: FBP reconstruction. TV: network term is not used. Network: TV term is not used. TV + Network: both TV and network terms are used.

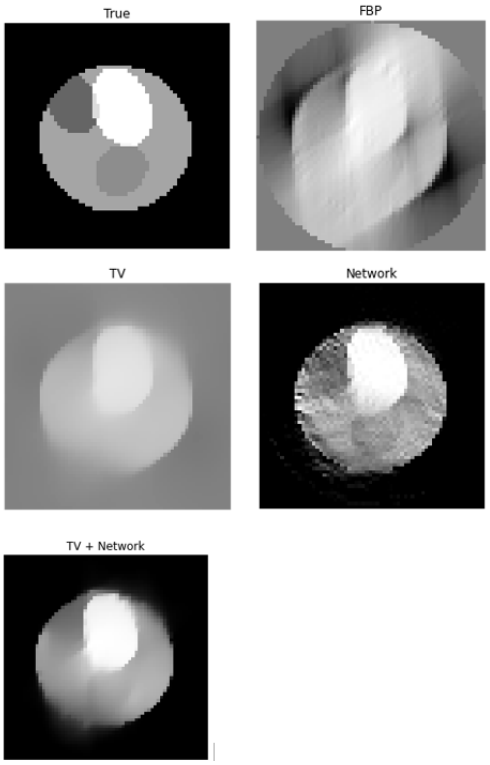

Figure 2: Simulation case 2.
True: True image; FBP: FBP reconstruction; TV: network term is not used; Network: TV term is not used; TV + Network: both TV and network terms are used.

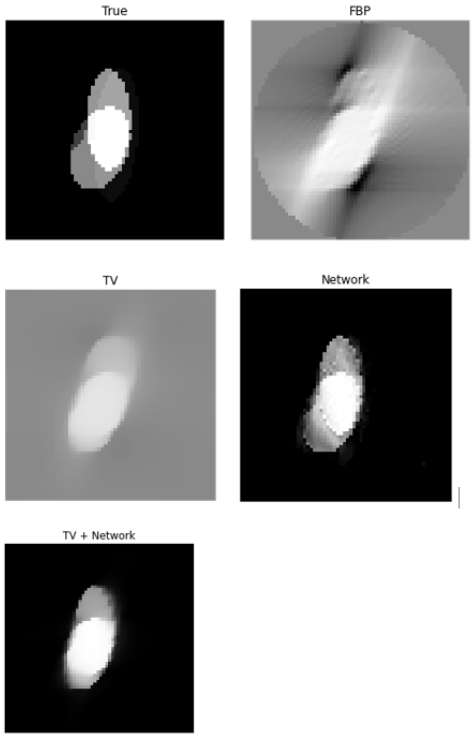

Figure 3: Simulation case 3.
True: True image; FBP: FBP reconstruction; TV: network term is not used; Network: TV term is not used; TV + Network: both TV and network terms are used.

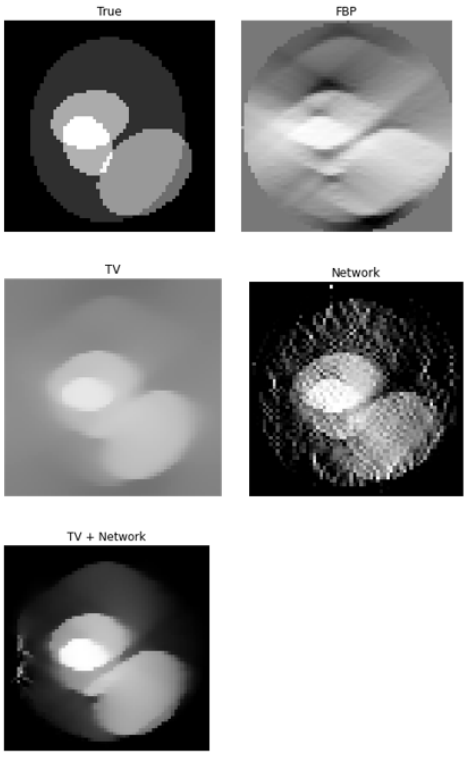

Figure 4: Simulation case 4.
True: True image; FBP: FBP reconstruction; TV: network term is not used; Network: TV term is not used; TV + Network: both TV and network terms are used.

Scanning angle = 60°

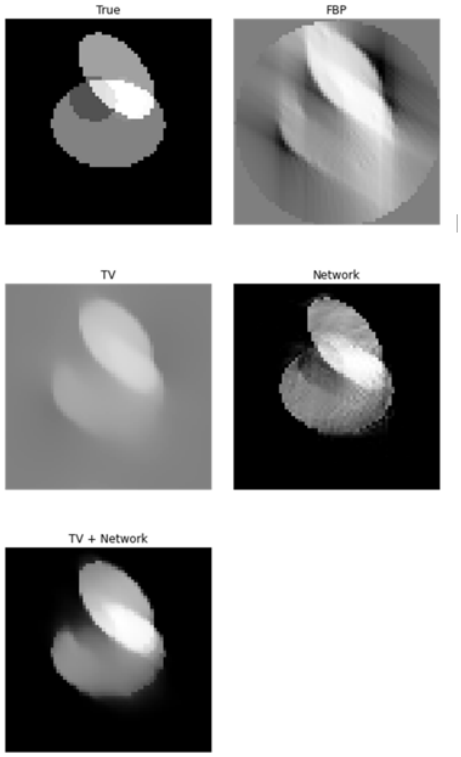

Figure 5: Simulation case 5.
True: True image; FBP: FBP reconstruction; TV: network term is not used; Network: TV term is not used; TV + Network: both TV and network terms are used.

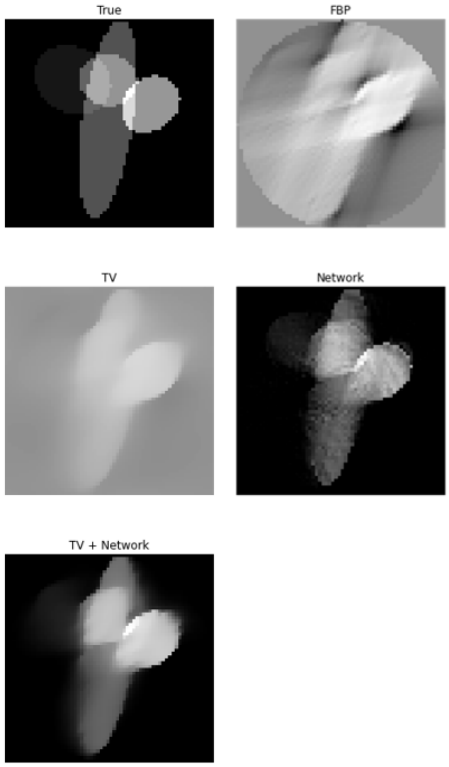

Figure 6: Simulation case 6.
True: True image; FBP: FBP reconstruction; TV: network term is not used; Network: TV term is not used; TV + Network: both TV and network terms are used.

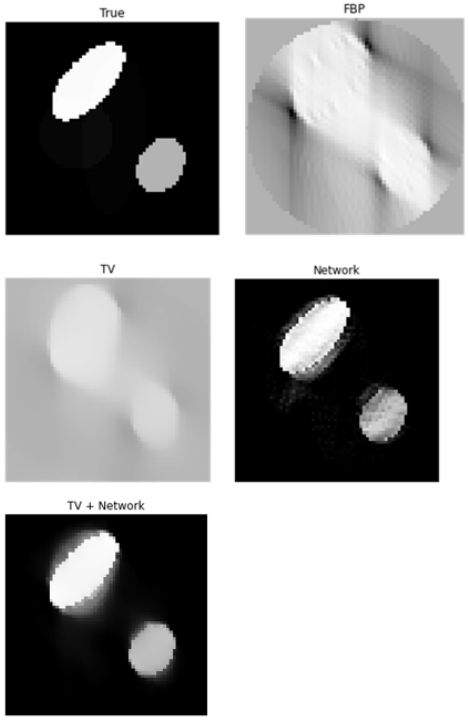

Figure 7: Simulation case 7.
True: True image; FBP: FBP reconstruction; TV: network term is not used; Network: TV term is not used; TV + Network: both TV and network terms are used

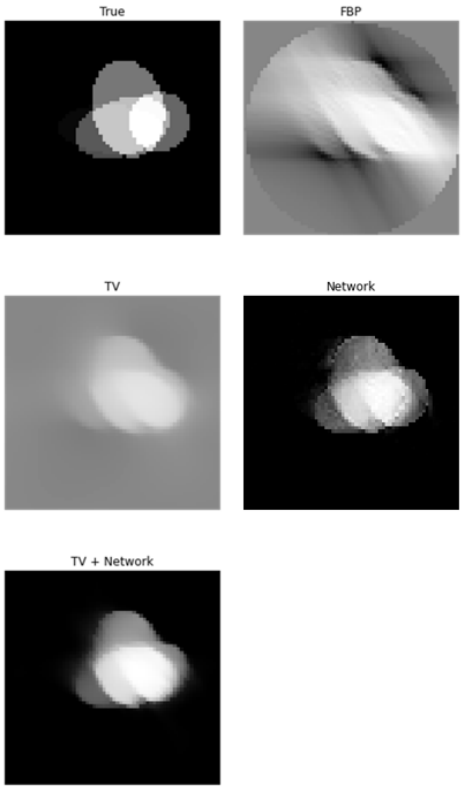

Figure 8: Simulation case 8.
True: True image; FBP: FBP reconstruction; TV: network term is not used; Network: TV term is not used; TV + Network: both TV and network terms are used.

Discussion and Conclusions

Image reconstruction with incomplete measurements such as limited-angle tomography is extremely ill-conditioned. Naïve reconstruction (e.g., using FBP) may not produce a useful image. Additional information (or prior knowledge of the object) must be used to assist with the reconstruction. This prior knowledge can be learned by a neural network from a large population of similar images. The extracted common features are stored in the network weights. In a neural network classifier, the input image is compared with the stored features, and the similarity score is the output. Thus, a network classifier is a good candidate for a Bayesian term in the objective function for image reconstruction.

Our computer simulations show the feasibility of using a neural network classifier as a Bayesian term in the objective function, as a supplement to the TV norm. The TV norm smooths image fluctuations, while the neural network better defines shapes and boundaries.

The limited-angle imaging cases (60° and 70°) are more severe than one encounters in reality. The final reconstruction still does not recover all edges in the original image. The effectiveness of the Bayesian terms is demonstrated by computer simulation examples.

Funding

This research was funded by NIH, grant number 2R15EB024283-03

References

1. Zeng GL. Medical Image Reconstruction: From Analytical and Iterative Methods to Machine Learning. Walter de Gruyter GmbH & Co KG, 2023.
2. Jaju PP, Jaju SP. Clinical utility of dental cone-beam computed tomography: current perspectives. Clin Cosmet Investig Dent. 2014; 6: 29-43.
3. Al-Rawi B, Hassan B, Vandenberge B, et al. Accuracy assessment of three-dimensional surface reconstructions of teeth from cone beam computed tomography scans. J Oral Rehabil. 2010; 37: 352-358.
4. Baciut M, Hedesiu M, Bran S, et al. Pre-and postoperative assessment of sinus grafting procedures using cone-beam computed tomography compared with panoramic radiographs. Clin Oral Implants Res. 2013; 24: 512-516.
5. Hatamikia S, Biguri A, Kronreif G, et al. Optimization for customized trajectories in cone beam computed tomography. Med Phys. 2020; 47: 4786-4799.
6. Zaech JN, Gao C, Bier B, et al. Learning to avoid poor images: Towards task-aware C-arm cone-beam CT trajectories. Medical Image Computing and Computer Assisted Intervention–MICCAI 2019. 2019; 22: 11-19.
7. Thies M, Zäch JN, Gao C, et al. A learning-based method for online adjustment of C-arm Cone-beam CT source trajectories for artifact avoidance. Int J Comput Assist Radiol Surg. 2020; 15: 1787-1796.
8. Tuy HK. An inversion formula for cone-beam reconstruction. SIAM Journal on Applied Mathematics. 1983; 43: 546-552.
9. Sujlana PS, Mahesh M, Vedantham S, et al. Digital breast tomosynthesis: Image acquisition principles and artifacts. Clin Imaging. 2019; 55: 188-195.
10. Lai YC, Ray KM, Mainprize JG, et al. Digital breast tomosynthesis: technique and common artifacts. J Breast Imaging. 2020; 2: 615-628.
11. Vedantham S, Karellas A, Vijayaraghavan GR, et al. Digital breast tomosynthesis: state of the art. Radiology. 2015; 277: 663-684.
12. Marshall NW, Bosmans H. Performance evaluation of digital breast tomosynthesis systems: physical methods and experimental data. Phys Med Biol. 2022; 67: 22TR03.
13. Kan MWK, Leung LHT, Wong W, et al. Radiation dose from cone beam computed tomography for image-guided radiation therapy. Int J Radiat Oncol Biol Phys. 2008; 70: 272-279.
14. Perks FR, Lehmann J, Chen AM, et al. Comparison of peripheral dose from image-guided radiation therapy (IGRT) using kV cone beam CT to intensity-modulated radiation therapy (IMRT). Radiother Oncol. 2008; 89: 304-310.
15. Zhang W, Song Y, Chen Y, et al. Limited-range few-view CT: Using historical images for ROI reconstruction in solitary lung nodules follow-up examination. IEEE Transactions on Medical Imaging. 2017; 36: 2569-2577.
16. Lu Y, Zhao J, Wang G. Few-view image reconstruction with dual dictionaries. Phys Med Biol. 2012; 57: 173.
17. Han X, Bian J, Ritman EL, et al. Optimization-based reconstruction of sparse images from few-view projections. Phys Med Biol. 2012; 57: 5245-5273.
18. Abbas S, Min J, Cho S. Super-sparsely view-sampled cone-beam CT by incorporating prior data. J Xray Sci Technol. 2013; 21: 71-83.
19. Adelman Z, Joskowicz L. Deformable registration and region-of-interest image reconstruction in sparse repeat CT scanning. J Xray Sci Technol. 2020; 28: 1069-1089. http://www.ncrponline.org/
20. Mayo-Smith WW, Hara AK, Mahesh M, et al. How I do it: Managing radiation dose in CT. Radiology. 2014; 273: 657-672.
21. Donald P Frush, DP. Review of radiation issues for computed tomography. Semin Ultrasound CT MR. 2004; 25: 17-24.
22. Golding SJ, Shrimpton PC. Radiation dose in CT: Are we meeting the challenge? Br J Radiol. 2002; 75: 1-4.
23. Huda W. Radiation doses and risks in chest computed tomography examinations. Proc Am Thorac Soc. 2007; 4: 316-320.
24. Slovis TL. Children, computed tomography radiation dose, and the As Low As Reasonably Achievable (ALARA) concept. Pediatrics. 2003; 112: 971-972.
25. Morris JA. Low dose radiation and childhood cancer. J Clin Pathol. 1992; 45: 378.
26. Brody AS, Frush DP, Huda W, et al. Radiation risk to children from computed tomography. Pediatrics. 2007; 120: 677-682.

27. Cohen MD. Pediatric CT radiation dose: how low can you go? American Journal of Roentgenology. 2009; 192: 1292-1303.
28. Bertero M, Boccacci P, De Mol C. Introduction to inverse problems in imaging. CRC press. 2021.
29. Scherzer O. Handbook of mathematical methods in imaging. Springer Science & Business Media. 2010.
30. Bertero M, Piana, M. Inverse problems in biomedical imaging: modeling and methods of solution. Complex systems in biomedicine. 2006; 1-33.
31. Brooks RA, Di Chiro G. Theory of image reconstruction in computed tomography. Radiology. 1975; 117: 561-572.
32. Easton Jr RL. Fourier methods in imaging. John Wiley & Sons. 2010.
33. Clackdoyle R, Defrise M. Tomographic reconstruction in the 21st century. IEEE Signal Processing Magazine. 2010; 27: 60-80.
34. Davison ME. The ill-conditioned nature of the limited angle tomography problem. SIAM Journal on Applied Mathematics. 1983; 43: 428-448.
35. Bertero M, Lantéri H, Zanni L. Iterative image reconstruction: a point of view. Mathematical Methods in Biomedical Imaging and Intensity-Modulated Radiation Therapy (IMRT). 2008; 7: 37-63.
36. Oliva-García R, Marichal-Hernández JG, Gómez-Cárdenes Ó, et al. A fast but ill-conditioned formal inverse to Radon transforms in 2D and 3D. In Real-Time Image Processing and Deep Learning. 2022; 12102: 62-75.
37. Lu X, Sun Y, Yuan Y. Image reconstruction by an alternating minimisation. Neurocomputing. 2011; 74: 661-670.
38. Deng X, Yin L, Peng S, et al. An iterative algorithm for solving ill-conditioned linear least squares problems. Geodesy and Geodynamics. 2015; 6: 453-459.
39. Hart II VP. The application of tomographic reconstruction techniques to ill-conditioned inverse problems in atmospheric science and biomedical imaging. Utah State University. 2012.
40. Grünbaum FA. A study of Fourier space methods for 'limited angle' image reconstruction. Numerical Functional Analysis and Optimization. 1980; 2: 31-42.
41. Zhang Jian, ChenZhang J, Chen J, et al. Image compressive sensing recovery using adaptively learned sparsifying basis via L0 minimization. Signal Processing. 2014; 103: 114-126.
42. Hyder M, Mahata K. An approximate l0 norm minimization algorithm for compressed sensing. in 2009 IEEE International Conference on Acoustics, Speech and Signal Processing. 2009; 3365-3368.
43. Wei Z, Jianlin Zhang J, Xu Z, et al. Gradient projection with approximate L0 norm minimization for sparse reconstruction in compressed sensing. Sensors. 2018; 18: 3373.
44. Zeng L, Yu P, Pong TK. Analysis and algorithms for some compressed sensing models based on L1/L2 minimization. SIAM Journal on Optimization. 2021; 31: 1576-1603.
45. Nguyen TBT, Thi HAL, Le HM, et al. Dc approximation approach for ℓ0-minimization in compressed sensing. Advanced Computational Methods for Knowledge Engineering: Proceedings of 3rd International Conference on Computer Science, Applied Mathematics and Applications-ICCSAMA. 2015; 37-48.
46. Kabashima Y, Wadayama T, Tanaka T. A typical reconstruction limit for compressed sensing based on lp-norm minimization. J Stat Mech. 2009; L09003.
47. Doneva M, Börnert P, Eggers H, et al. Compressed sensing reconstruction for magnetic resonance parameter mapping. Magn Reson Med. 2010; 64: 1114-1120.
48. Li L, Fang Y, Liu L, et al. Overview of compressed sensing: Sensing model, reconstruction algorithm, and its applications. Appl Sci. 2020; 10: 5909.
49. Donoho DL. Compressed sensing. IEEE Transactions on information theory. 2006; 52: 1289-1306.
50. Pope G. Compressive Sensing: A Summary of Reconstruction algorithms. Master's thesis, ETH. 2009.
51. Shchukina A, Kasprzak P, Dass R, et al. Pitfalls in compressed sensing reconstruction and how to avoid them. J Biomol NMR. 2017; 68: 79-98.
52. Hollingsworth KG. Reducing acquisition time in clinical MRI by data undersampling and compressed sensing reconstruction. Phys Med Biol. 2015; 60: R297-322.
53. Chan RW, Ramsay EA, Cheung EY, et al. The influence of radial undersampling schemes on compressed sensing reconstruction in breast MRI. Magn Reson Med. 2012; 67: 363-377.
54. Peyre G. Best basis compressed sensing. IEEE Transactions on Signal Processing. 2010; 58: 2613-2622.
55. Pilastri AL, Tavares JMRS. Reconstruction algorithms in compressive sensing: An overview. Proceedings of the Doctoral Symposium in Informatics and Telecommunications Engineering. 2016; 127-137.
56. Baron CA, Dwork N, Pauly JM, et al. Rapid compressed sensing reconstruction of 3D non-Cartesian MRI. Magn Reson Med. 2018; 79: 2685-2692.
57. Wei SJ, Zhang XL, Shi J, et al. Sparse reconstruction for SAR imaging based on compressed sensing. Progress in Electromagnetics Research. 2010; 109: 63-81.
58. Sánchez AA. Estimation of noise properties for TV-regularized image reconstruction in computed tomography. Phys Med Biol. 2015; 60: 7007-7033.
59. Sidky EY, Pan X. Image reconstruction in circular cone-beam computed tomography by constrained, total-variation minimization. Phys Med Biol. 2008; 53: 4777.
60. Zhang J, Li S, Lipson E, et al. Image quality comparison of reconstruction using total variation-based regularizers. IEEE Symposium on Nuclear Science (NSS/MIC). 2014; 1-3.
61. Fessler JA. Iterative methods for image reconstruction. ISBI Tutorial. 2006.
62. Fessler JA. Optimization methods for magnetic resonance image reconstruction: Key models and optimization algorithms. IEEE Signal Process Mag. 2020; 37: 33-40.

63. Chen Z, Jin X, Li L, et al. A limited-angle CT reconstruction method based on anisotropic TV minimization. Phys Med Biol. 2013; 58: 2119-2141.
64. Liu Y, Ma J, Fan Y, et al. Adaptive-weighted total variation minimization for sparse data toward low-dose x-ray computed tomography image reconstruction. Phys Med Biol. 2012; 57: 7923.
65. Chen B, Bian Z, Zhou X, et al. A new Mumford–Shah total variation minimization based model for sparse-view x-ray computed tomography image reconstruction. Neurocomputing (Amst). 2018; 285: 74-81.
66. Yu G, Li L, Gu J, et al. Total variation based iterative image reconstruction. CVBIA'05: Proceedings of the First international conference on Computer Vision for Biomedical Image Applications. 2005; 526-534.
67. Zhang Y, Zhang WH, Chen H, et al. Few-view image reconstruction combining total variation and a high-order norm. International Journal of Imaging Systems and Technology. 2013; 23: 249-255.
68. Tian Z, Jia X, Yuan K, et al. Low-dose CT reconstruction via edge-preserving total variation regularization. Phys Med Biol. 2011; 56: 5949-5967.
69. Zhang Z, Chen B, Xia D, et al. Directional-TV algorithm for image reconstruction from limited-angular-range data. Med Image Anal. 2021; 70: 102030.
70. Zhang HM, Dong B. A review on deep learning in medical image reconstruction. J Oper Res Soc China. 2020; 8: 311-340.
71. Wang G, Ye JC, Mueller K, et al. Image reconstruction is a new frontier of machine learning. IEEE transactions on medical imaging. 2018; 37: 1289-1296.
72. Hammernik K, Knoll F. Machine learning for image reconstruction. Handbook of Medical Image Computing and Computer Assisted Intervention. 2020; 25-64.
73. Ahishakiye E, Van Gijzen MB, Tumwiine J, et al. A survey on deep learning in medical image reconstruction. Intelligent Medicine. 2021; 1: 118-127.
74. Ravishankar S, Ye JC, Fessler JA. Image reconstruction: From sparsity to data-adaptive methods and machine learning. Proc IEEE Inst Electr Electron Eng. 2019; 108: 86-109.
75. Yedder HB, Cardoen B, Hamarneh G. Deep learning for biomedical image reconstruction: A survey. Artificial Intelligence Review. 2021; 54: 215-251.
76. Yaqub M, Feng J, Arshid K, et al. Deep learning-based image reconstruction for different medical imaging modalities. Comput Math Methods Med. 2022; 8750648.
77. Maier A, Syben C, Lasser T, et al. A gentle introduction to deep learning in medical image processing. Z Med Phys. 2019; 29: 86-101.
78. Razzak MI, Naz S, Zaib A. Deep learning for medical image processing: Overview, challenges and the future. Classification in BioApps. 2018; 323-350.
79. Haq N, Johnson P, Maier A, et al. Machine Learning for Medical Image Reconstruction. Springer International Publishing. 2021.
80. Montalt-Tordera J, Muthurangu V, Hauptmann A, et al. Machine learning in magnetic resonance imaging: image reconstruction. Phys Med. 2021; 83: 79-87.
81. Wang G, Ye JC, De Man B. Deep learning for tomographic image reconstruction. Nature Machine Intelligence. 2020; 2: 737-748.
82. Maier A, Köstler H, Heisig M, et al. Known operator learning and hybrid machine learning in medical imaging—a review of the past, the present, and the future. Prog Biomed Eng. 2022; 4: 022002.
83. Muckley MJ, Riemenschneider B, Radmanesh A, et al. Results of the 2020 fastMRI challenge for machine learning MR image reconstruction. IEEE Transactions on Medical Imaging. 2021; 40: 2306-2317.
84. Lee H, Huang C, Yune S, et al. Machine friendly machine learning: interpretation of computed tomography without image reconstruction. Scientific Reports. 2019; 9: 15540.
85. Wang G, Jacob M, Mou X, et al. Deep tomographic image reconstruction: yesterday, today, and tomorrow—editorial for the 2nd special issue 'Machine Learning for Image Reconstruction'. IEEE Transactions on Medical Imaging. 2021; 40: 2956-2964.
86. Liu H, Xu J, Wu Y, et al. Learning deconvolutional deep neural network for high resolution medical image reconstruction. Information Sciences. 2018; 468: 142-154.
87. Saravanan S, Juliet S. Deep medical image reconstruction with autoencoders using deep Boltzmann machine training. EAI Endorsed Transactions on Pervasive Health and Technology. 2020; 6.
88. Gjesteby L, Yang Q, Xi Y, et al. Deep learning methods to guide CT image reconstruction and reduce metal artifacts. Medical Imaging 2017: Physics of Medical Imaging. 2017; 10132: 752-758.
89. Arndt C, Güttler F, Heinrich A, et al. Deep learning CT image reconstruction in clinical practice. Rofo. 2021; 193: 252-261.
90. Güngör A, Dar SUH, Öztürk Ş, et al. Adaptive diffusion priors for accelerated MRI reconstruction. Medical Image Analysis. 2023; 88: 102872.
91. Xie Y, Li Q. Measurement-conditioned denoising diffusion probabilistic model for under-sampled medical image reconstruction. Medical Image Computing and Computer-Assisted Intervention. 2022; 655-664.
92. Jayakumar N, Hossain T, Zhang M. SADIR: shape-aware diffusion models for 3D image reconstruction. Shape in Medical Imaging. 2023; 287-300.
93. Peng C, Guo P, Zhou SK, et al. Towards performant and reliable undersampled MR reconstruction via diffusion model sampling. Medical Image Computing and Computer-Assisted Intervention. 2022; 623-633.
94. Bhadra S, Kelkar VA, Brooks FJ, et al. On hallucinations in tomographic image reconstruction. IEEE Transactions on Medical Imaging. 2021; 40: 3249-3260.

95. Stephens K. Investigating hallucinations in medical imaging. AXIS Imaging News. 2022.

96. Wang K, Oramas J, Tuytelaars T. Multiple exemplars-based hallucination for face super-resolution and editing. Proceedings of the Asian Conference on Computer Vision. 2020.

97. Sun J, Zhu J, Tappen MF. Context-constrained hallucination for image super-resolution. 2010 IEEE Computer Society Conference on Computer Vision and Pattern Recognition. 2010; 231-238.

98. Zhao Zh, Sun Y, Cong P. Sparse-view CT reconstruction via generative adversarial networks. 2018 IEEE Nuclear Science Symposium and Medical Imaging Conference Proceedings (NSS/MIC). 2018; 1-5.

99. Zhao J, Huang Q, Liang D, et al. Deep learning for medical image reconstruction: Focus on MRI, CT and PET. Deep Learning for Medical Image Analysis. 2024; 247-278.

100. https://www.tensorflow.org/api_docs/python/tf/GradientTape

101. Zeng GL. Better Than the Total Variation Regularization. Int J Biomed Res Prac. 2024; 4: 1-4.

102. Zeng GL. Neural network guided sinogram-domain iterative algorithm for artifact reduction. Med Phys. 2023; 50: 5410-5420.

103. https://www.tensorflow.org/api_docs/python/tf/GradientTape